Towards an Ankle-Foot Orthosis Powered by a Dielectric Elastomer Actuator

David P. Allen[a], Ryan Little[b], Joshua Laube[b], Jeremy Warren[c], Walter Voit[d], Robert D. Gregg[e,*]

[a]*Departments of Mechanical Engineering and Bioengineering, The University of Texas at Dallas, 800 W Campbell Rd, Richardson, TX 75080*
[b]*Department of Mechanical Engineering, The University of Texas at Dallas, 800 W Campbell Rd, Richardson, TX 75080*
[c]*Department of Bioengineering, The University of Texas at Dallas, 800 W Campbell Rd, Richardson, TX 75080*
[d]*Departments of Mechanical Engineering, Bioengineering, and Materials Science and Engineering, The University of Texas at Dallas, 800 W Campbell Rd, Richardson, TX 75080*
[e]*Department of Electrical Engineering and Computer Science, Robotics Institute, University of Michigan, Ann Arbor, MI 48109, USA*

Abstract

Foot drop is the inability to dorsiflex the ankle (raise the toes) due to neuromuscular impairment, and this common condition can cause trips and falls. Current treatments for chronic foot drop provide dorsiflexion support, but they either impede ankle push off or are not suitable for all patients. Powered ankle-foot orthoses (AFOs) can counteract foot drop without these drawbacks, but they are heavy and bulky and have short battery life. To counteract foot drop without the drawbacks of current treatments or powered AFOs, we designed and built an AFO powered by dielectric elastomer actuators (DEAs), a type of artificial muscle technology. This paper presents our design and the results of benchtop testing. We found that the DEA AFO can provide 49 % of the dorsiflexion support necessary to raise the foot. Further, charging the DEAs reduced the effort that would be required for plantarflexion compared to that with passive DEA behavior, and this operation could be powered for 7000 steps or more in actual operation. DEAs are a promising approach for building an AFO that counteracts foot drop without impeding plantarflexion, and they may prove useful for other powered prosthesis and orthosis designs.

1. Background on foot drop remedies

Foot drop is the condition of not being able to dorsiflex the ankle (raise the toes) properly due to a neuromuscular impairment [1]. People with foot drop are prone to trip and fall because their toes drag on the ground and catch on obstacles, and their

*Corresponding author
Email address: rdgregg@umich.edu, rgregg@ieee.org (Robert D. Gregg)

affected foot slaps onto the ground after heel contact. Foot drop can be caused by stroke or injuries that affect the peroneal nerve, so people with foot drop are often otherwise healthy and have the ability to plantarflex their affected ankle (lower the toes).

Current treatments for chronic foot drop improve mobility, but they have drawbacks. Passive ankle-foot orthoses (AFOs) are essentially springs that lift a patient's foot so that there is sufficient toe clearance while the leg is swinging. These common devices are effective, lightweight, simple, and cheap. However, the dorsiflexion assistance they provide comes at the cost of making plantarflexion more difficult. Functional electrical stimulation devices do not have this drawback. They provide dorsiflexion by applying neural stimulation to the patient's peroneal nerve causing the ankle dorsiflexors to contract and lift the toes [1]. They deactivate during push-off allowing the ankle to plantarflex freely. However, they only work for a limited patient population because they rely on functional muscles and nerves, and not all patients can tolerate the stimulation sensation.

Powered AFOs can relieve foot drop symptoms without the drawbacks of current treatments, but AFOs powered by electric motors and pneumatic actuators have their own drawbacks. These drawbacks are weight, bulk, noise, and short operational endurance (unless using a tethered power supply). An early powered AFO driven by an electric motor provided dorsiflexion assistance to increase toe clearance and reduce foot slap and minimized plantarflexion impedance during push-off [2]. It worked so well that study participants with foot drop preferred the device over passive AFOs, and one participant "remarked that the [powered AFO] made walking 'almost subconscious, like normal walking' " [2]. However, this AFO had a mass of 2.6 kg, required a tethered power supply, and was too bulky for everyday use. Two recent AFOs powered by electric motors are much lighter (masses of 1.2 kg [3] and 1.0 kg [4]) and are battery powered. However, a study using the 1.0 kg, powered AFO indicated that even the 0.5 kg that this design placed on the wearer's ankle might have detrimental gait effects [5]. Another design for an untethered, powered AFO used a pneumatic actuator powered by a carbon dioxide tank worn on the user's belt [6]. It was also bulky and heavy (1.9 kg AFO + 1.2 kg on belt), and its carbon dioxide supply was only sufficient for 1914 steps. Later works showed that this AFO's carbon dioxide consumption could be reduced by 25 % by using an accumulator to recycle exhaust gasses [7], or reduced by 91 % by using proportional valves instead of solenoid valves [8], so a revision of this AFO design could achieve greater operational endurance. Another pneumatic powered AFO placed merely 0.94 kg on the wearer's ankle and was powered by an electric compressor worn on the user's waist [9]. A version of the compressor had a mass of 2.6 kg with a battery that would power it for an hour (yielding 2160 steps at 0.6 Hz) [10]. This compressor emitted a sound level of 65 dB, which would make the AFO wearer undesirably conspicuous. The sound levels of the other AFOs mentioned in this paragraph were not reported, but their transmissions and valves probably make too much noise for practical everyday use.

A question thus arises: how can we obtain the benefits of powered AFOs without the noise, bulk, and inefficiency that normally accompany them? Doing so would improve the quality of life for people with foot drop, and it could also lead to improvements in other prosthesis and orthosis designs.

Clutched-spring and semi-active AFOs could be quieter, lighter, and less energy-hungry than powered AFOs, but none of the designs reported to date provide dorsiflexion

assistance during swing without impeding push off. A clutched-spring AFO reduced the metabolic cost of walking without using actuators or doing net positive work [11]. This remarkable achievement inspired two other clutched-spring AFOs with mechanical improvements to the design. One of these had a slimmer form factor that could be worn under clothing [12]. The other was able to vary its stiffness by changing the number of springs engaged by its electrostatic clutches [13]. However, these AFOs only provide plantarflexion assistance, not dorsiflexion assistance. Two semi-active AFOs used variable dampers to prevent foot drop [14, 15], but these designs impede push off like passive AFOs.

Dielectric elastomer actuators (DEAs), a type of artificial muscle, may be able to power an AFO that provides dorsiflexion assistance without impeding plantarflexion, and have been suggested for this very application [16, 17]. When charged with a constant voltage, DEAs soften and expand due to electrostatic forces [18, 19]. However, DEAs typically require voltages in the kilovolt range to create sufficiently strong electrostatic forces for operation making them challenging to work with. Further, the performance of many DEAs is hampered by the effects of viscoelasticity, the material behavior that causes stress to increase with strain and strain rate [20], which slows their motion and makes precise control more challenging.

The research question that this work seeks to answer is: how can we design a DEA-powered AFO that will relieve foot drop symptoms with less mass, volume, noise, and energy consumption than electric and pneumatic powered AFOs? To answer this question, we analyzed the application requirements for a DEA AFO that provides foot drop assistance and built a proof of concept device. This paper reports the results of our analysis (§ 2), describes the device (§ 3), and reports the methods (§ 4) and results (§ 5) of our benchtop tests.

2. Analysis of application requirements

Our analysis of application requirements guides the design of our DEA AFO. It starts by examining how the effects of foot drop on walking gait can be counteracted. This analysis leads to the overall structure of our DEA AFO. Then, the geometry of the DEA AFO is analyzed to determine how to minimize the force and actuation stretch required from the DEA. Finally, the function of a charge recovery system is analyzed to help increase the AFO's battery life.

2.1. Counteracting foot drop

During normal-speed walking on level ground, the ankle flexes cyclically over a period of approximately 1 s [21] (Figure 1, Ankle angle [22]). The walking gait cycle starts at *heel strike*, the moment when the foot touches the ground, in a phase called *loading response*. During loading response, the ankle plantarflexes, lowering the toes until they contact the ground at the moment of *toe contact*, which begins the *foot flat* phase. During foot flat, the shank pivots forward over the ankle. The moment of *heel off*, when the heel leaves the ground, starts the *push off* phase. During push off, the ankle plantarflexes rapidly. Push off ends and the swing phase begins at the moment of *toe off*, when the toes leave the ground. At the start of *swing*, the ankle dorsiflexes,

raising the toes so that the foot is clear of the ground as it swings forward for the next gait cycle that begins at heel strike.

An AFO can counteract foot drop without impeding plantarflexion by mimicking the function of the ankle dorsiflexor muscles. Foot drop is an impairment of the ankle dorsiflexor muscles that allows the ankle to plantarflex too quickly during loading response and reduces toe clearance during swing, possibly causing audible foot slap, trips, and falls [21]. Passive AFOs counteract foot drop by exerting dorsiflexion torque throughout the gait cycle, which impedes plantarflexion. Impeding plantarflexion is undesirable because it increases the effort that the ankle plantarflexor muscles exert during push off to achieve normal ankle motion. Accordingly, to counteract foot drop without impeding plantarflexion, an AFO should provide dorsiflexion torque during loading response, relax during push off, and provide dorsiflexion torque again during swing, which is nearly the same pattern as normal dorsiflexor muscle activity [21].

A DEA behaves like a variable-stiffness spring mechanically and a capacitor electrically. The fundamental DEA element is an elastomer film sandwiched between a pair of stretchable electrodes, which forms a stretchable capacitor (Figure 2). In this work, the DEA is free to displace in the length (l_1) direction, but its width l_2 is fixed by stiffening fibers. The DEA's load F is applied in the length direction, and the DEA responds to its load like a spring: it lengthens until its internal elastic force balances the load. When a constant voltage V is applied across the electrodes, charge Q flows onto the electrodes in proportion to the DEA's capacitance. These charges create electrostatic forces that act to compress the DEA's thickness l_3 and expand its area. These forces cause the DEA's no-load length to increase. They also cause the DEA to soften with respect to the load, so that a given force lengthens the DEA more than it would with no voltage applied. Thus, the DEA can be thought of as a variable-stiffness spring that decreases its stiffness and increases its no-load length when charged with a constant voltage [23].

The core of our DEA AFO design is a DEA strap that connects the foot near the toes to the shank near the knee (Figure 3). The DEA passively holds the foot up (dorsiflexed) to the maximum angle experienced during normal walking. This arrangement leads to two benefits. First, passive dorsiflexion support means that the AFO can provide toe-lift support even when powered off, so it can still relieve foot drop like a passive AFO even if it runs out of battery power. Second, attaching the DEA to the foot in front of (anterior to) the ankle makes the DEA support the weight of the foot with a tensile force, so there is no concern about it buckling under load like there would be if it was loaded with a compressive force.

Our DEA AFO is controlled with a single sensor for detecting gait timing: a toe contact sensor. The AFO should be stiff during loading response to prevent foot slap, soft during push off to allow push off, and stiff during swing to prevent toe dragging (Figure 1, DEA stiffness). Accordingly, the voltage on the DEA should be low during loading response, high during push off, and low during swing. The stiffness during foot flat is not very important, so we use this phase to ramp up the voltage on the DEA, which wastes less energy than stepping up the voltage [24]. The moments for changing voltage correspond to the moments of toe contact and toe off, and these can be detected with a toe contact sensor such as a pressure switch or force-sensing resistor. Thus, the AFO will automatically adapt to changes in the wearer's gait speed because the sensor will detect when the toes are on the ground and voltage should be applied to the DEA,

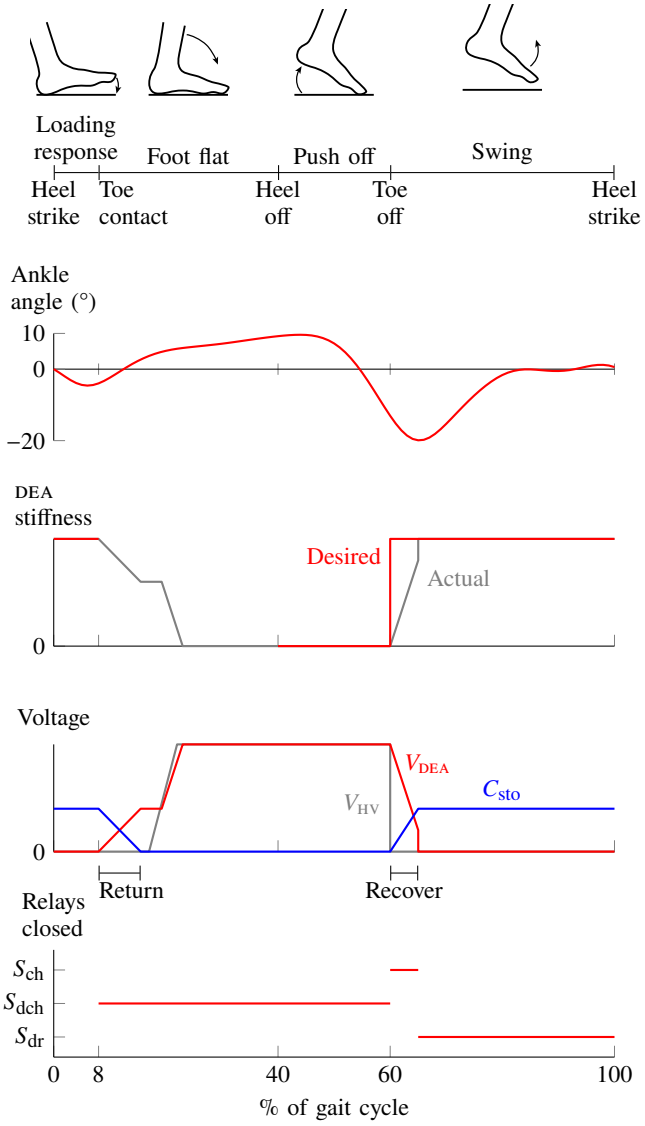

Figure 1: The DEA AFO provides dorsiflexion support to relieve foot drop symptoms by stiffening during swing and loading response, and it avoids impeding push off by softening during push off. To increase battery life, the DEA AFO's charge recovery system recovers charge from the DEA at the start of swing and returns it at the start of foot flat.

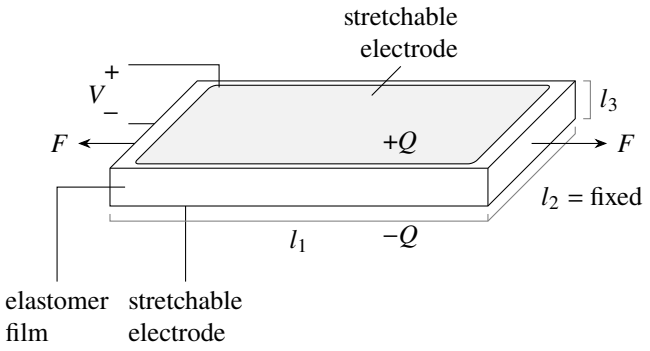

Figure 2: A DEA consists of an elastomer film sandwiched between a pair of stretchable electrodes. In the width-constrained configuration used in this work, a DEA is loaded with force F along its length l_1, its width l_2 is fixed by stiffening fibers, its thickness l_3 is constrained by the elastomer film's constant volume, and charge Q is stored on the electrodes corresponding to voltage V across the electrodes.

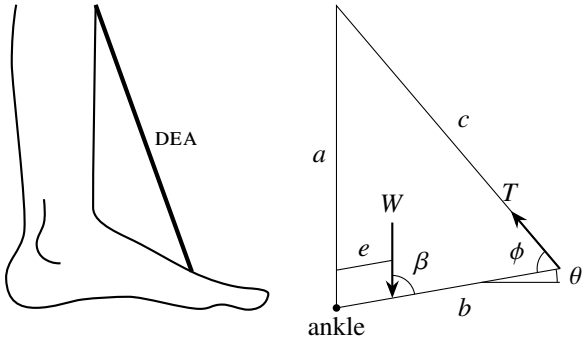

Figure 3: The core of our DEA AFO design is a DEA strap that lifts the toes. To determine actuation stretch required from the DEA, the geometry of the DEA AFO is modeled by a triangle with sides a and b representing the distances from the strap's attachment points to the ankle and side c representing the length of the DEA. To determine the force required from the DEA, the DEA's loading is modeled as foot weight W and DEA tension T acting on the lever arm b.

and when the toes are off the ground and the DEA should be discharged. This approach requires placing a sensor in the user's shoe, but if doing so is undesirable, other timing control methods are possible such as using an inertial measurement unit to measure gait phase as done for robotic prosthetic legs [25, 26].

2.2. Minimizing force and actuation stretch

The goals for this section are to 1) determine where to place the DEA's foot and leg connections so as to minimize the force and actuation stretch required from the DEA, and 2) to calculate the force and actuation stretch requirements for the DEA. To do so, the geometry of the AFO is modeled and analyzed to determine the effect of connection placement on the force and actuation stretch requirements. Then, connection placements are selected based on the results of the analysis in order to achieve a compromise between the goals of minimizing actuation stretch and minimizing force. Finally, the model is used with the selected connection placements to calculate the force and actuation stretch requirements for the DEA.

We can calculate the required actuation stretch for the DEA by modeling the AFO's geometry as a triangle (Figure 3). In this triangle, a and b are the distances from the ankle joint to the DEA's shank and foot attachments respectively, and θ is the ankle angle, where $\theta = 0$ means the ankle is perpendicular to the shank. Length c represents the length of the DEA, which includes active stretchable length c_{DEA} and length c_{stiff} that represents the unstretchable portions of the DEA such as its mounting connectors, so we have

$$c_{\text{DEA}} = c - c_{\text{stiff}}. \tag{1}$$

The DEA's actuation stretch S is the ratio of its maximum length to its minimum length, which occur at the minimum and maximum values of θ:

$$S = \frac{c_{\text{DEA, max}}}{c_{\text{DEA, min}}} = \frac{c_{\text{DEA}}(\theta_{\text{min}})}{c_{\text{DEA}}(\theta_{\text{max}})}. \tag{2}$$

The length c_{DEA} can be calculated by using the law of cosines and simplifying with trigonometry and algebra:

$$c_{\text{DEA}} = \sqrt{a^2 + b^2 - 2ab\sin(\theta)} - c_{\text{stiff}}. \tag{3}$$

We can calculate the force the DEA must support from summing the moments about the ankle due to the DEA force and the foot's weight (Figure 3). The foot weight W acts at angle β at the position of the foot's center of mass, which is distance e away from the ankle. The DEA force T acts at angle ϕ at the DEA's foot connection point, which is distance b from the ankle. The sum of moments about the ankle is:

$$\begin{aligned}\sum M_{\text{ankle}} &= Tb\sin(\phi) - We\sin(\beta) \\ &= \left(\frac{Tab}{\sqrt{a^2 + b^2 - 2ab\sin(\theta)}} - We\right)\cos(\theta) = 0\end{aligned} \tag{4}$$

Because $-90° < \theta < 90°$, $\cos(\theta)$ is greater than zero, so we must have

$$T = \frac{\sqrt{a^2 + b^2 - 2ab\sin(\theta)}}{ab}We. \tag{5}$$

Table 1: Parameters used for calculating AFO specifications

Quantity	Symbol	Value
distance from ankle to		
leg attachment point	a	1 cm to 35 cm
foot attachment point	b	1 cm to 16 cm
foot center of mass	e	8 cm
stiff portion of DEA	c_{stiff}	9.2 cm
ankle angle	θ	−20° to 10°
foot weight	W	12 N

We use $\theta = \theta_{\max}$ for calculating design requirements to determine the force the DEA must exert to hold the foot at its greatest angle.

The connection placements of $a = 35\,\text{cm}$ and $b = 5\,\text{cm}$ achieve a compromise between minimizing actuation stretch and force requirements. We analyzed the effect of connection placements on force and actuation stretch numerically using the parameters in Table 1 in Equations (2) to (4). Actuation stretch can be minimized by either minimizing a and maximizing b, or maximizing a and minimizing b (Figure 4). In contrast, force is minimized by maximizing both a and b. We chose to achieve a compromise between these goals by first setting a to its maximum value (35 cm) because maximizing a minimizes both force and actuation stretch. Then we selected $b = 5\,\text{cm}$ because it resulted in the minimum force requirement for an actuation stretch which we expected to be attainable by our DEA design. Plugging $a = 35\,\text{cm}$ and $b = 5\,\text{cm}$ into Equations (2) to (4) yields the force and actuation stretch requirements for the AFO's DEA:

$$S = 1.1 \text{ (unitless), and} \tag{6}$$

$$T = 19\,\text{N}. \tag{7}$$

2.3. Increasing battery life with charge recovery

One of the application requirements is that the AFO run on a battery. Ideally, the battery would last long enough for a full day of walking (6000 to 10 000 steps [27]). There are many ways to help increase the battery life of the AFO with common electrical engineering practices. Here, we concentrate on a practice that is less known, designing a charge recovery system to decrease the amount of energy needed from the high-voltage DC-DC converter. To do so, this section will first explain why a charge recovery system helps improve the energy efficiency of a DEA actuation system, and then it will analyze how the recovery system should be designed.

A charge recovery system can increase the AFO's battery life. If a DEA is held at a constant voltage while being stretched to a larger area, half of the electrical energy that flows into the DEA during the stretching is converted to mechanical work, and

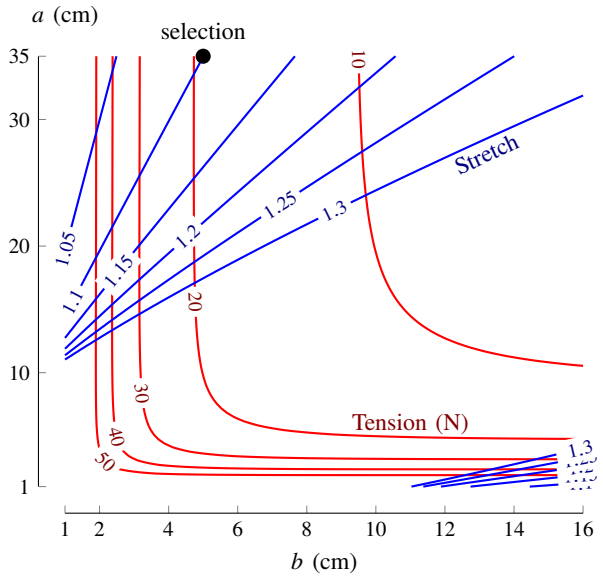

Figure 4: The selection of $a = 35\,\text{cm}$ and $b = 5\,\text{cm}$ for the connection placements achieves a compromise between minimizing actuation stretch and force requirements.

the other half is stored as electrical energy in the DEA [18, 28]. Often, the stored electrical energy is subsequently drained through a resistor so that the DEA will return to its uncharged shape, resulting in energy efficiency of no more than 50 %. This 50 % efficiency limit comes from the fundamental energy conversion process, and does not account for other loss mechanisms, which reduce energy efficiency further [28]. This limit can be removed by using a charge recovery system to transfer the electrical energy off the DEA and store it elsewhere for later use.

Our charge recovery system (Figure 5) uses a high-voltage capacitor bank to recover charge from the AFO's DEA. It recovers charge from the DEA by closing the charge relay S_{ch} when the capacitor bank C_{sto} is at a lower voltage than the DEA. It returns charge to the DEA by closing the discharge relay S_{dch} when the capacitor bank is at a higher voltage than the DEA. This charge recovery method avoids losses incurred in converting the DEA's electrical energy to a low voltage for storage in a battery or low-voltage capacitor [29, 30].

A capacitive charge recovery system must have inductance to recover more than 25 % of the energy stored on a DEA. If a charged capacitor is connected directly to an uncharged capacitor, charge will flow from the first capacitor to the second until their voltages equalize. This process will dissipate at least half of the energy originally stored on the first capacitor [31], and no more than 25 % of the original energy will be stored in the second capacitor. Therefore, if the inductance L in our charge recovery system was zero, then no more than 25 % of the energy stored in the DEA could be transferred from the DEA to the capacitor bank. The energy loss occurs because the kinetic energy of the moving charges (the difference between the electrical potential energy in the

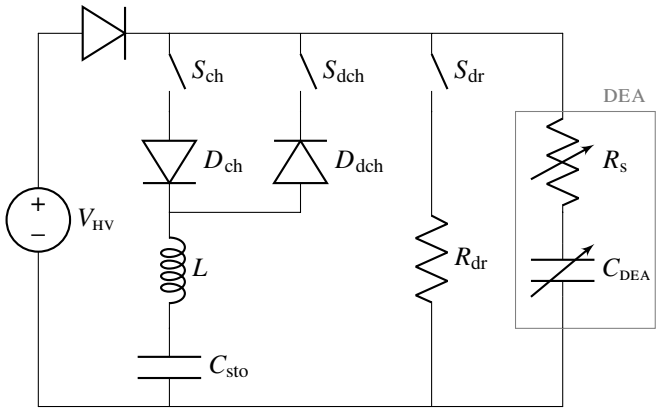

Figure 5: The DEA AFO's high-voltage power system features a charge recovery system to reduce the amount of energy needed from the high-voltage DC-DC converter to charge the DEA. The charge recovery system recovers charge from the DEA by closing S_{ch}, and it returns charge to the DEA by closing S_{dch}. The system can also drain the DEA by closing S_{dr}.

original capacitor and that in the two-capacitor system) is dissipated in a variety of possible ways [31], rather than stored. An inductor placed in series between the two capacitors will store the kinetic energy of the moving charges and then release it to the second capacitor, so the second capacitor can receive all of the energy originally stored on the first capacitor assuming there is no resistance [30]. Because of this principle, we have an inductor bank L in series with the capacitor bank. If the inductor bank is chosen so that the recovery circuit is underdamped, then the inductor bank will keep current flowing once the DEA and capacitor bank have the same voltage, so the capacitor bank will end up with a greater voltage than the DEA. The charge diode D_{ch} prevents the charge from flowing back towards the DEA. The charge recovery system can later transfer charge from the capacitor bank to the DEA by closing the discharge relay S_{dch}.

The charge recovery system needs to recover as much energy as possible from the DEA. Accordingly, we derive energy recovery as a function of the capacitance and inductance of the capacitor and inductor banks respectively as follows. Applying Kirchoff's voltage law to the loop through C_{DEA}, S_{ch}, D_{ch}, L, and C_{sto} yields the following equation:

$$\frac{Q_{DEA}}{C_{DEA}} = L\ddot{Q}_{sto} + R_s\dot{Q}_{sto} + \frac{Q_{sto}}{C_{sto}}, \tag{8}$$

where D_{ch} is assumed to have negligible voltage drop. If this loop is isolated from the rest of the circuit (i.e., S_{dch} and S_{dr} open, $V_{HV} = 0$), then the total charge in the loop Q_T is

$$Q_T = Q_{DEA} + Q_{sto}, \tag{9}$$

and Equation (8) simplifies to

$$V_0 = L\ddot{Q}_{sto} + R_s\dot{Q}_{sto} + \frac{Q_{sto}}{C}, \tag{10}$$

where

$$C = \frac{C_{\text{DEA}} C_{\text{sto}}}{C_{\text{DEA}} + C_{\text{sto}}} \tag{11}$$

is the total capacitance of the loop and $V_0 = {}^{Q_T}/_{C_{\text{DEA}}}$ is the voltage that the DEA is charged to at the moment that the charge switch is closed. Equation (10) is a second-order differential equation with a constant forcing term. The circuit must be underdamped for efficient energy recovery, so we must have

$$L > \frac{R_s^2 C}{4}. \tag{12}$$

Solving with the method of undetermined coefficients and the initial conditions $Q_{\text{sto}}(t = 0) = 0$, and $\dot{Q}_{\text{sto}}(t = 0) = 0$ yields

$$Q_{\text{sto}} = V_0 C \left[1 - e^{-\alpha t}\left(\frac{\alpha}{\omega}\sin(\omega t) + \cos(\omega t)\right)\right], \tag{13}$$

where

$$\alpha = \frac{R_s}{2L}, \text{ and } \omega = \sqrt{\frac{1}{LC} - \frac{R_s^2}{4L^2}}. \tag{14}$$

Q_{sto} reaches its maximum value when $\dot{Q}_{\text{sto}} = 0$, which occurs when $t = k\pi/\omega$, where k is a positive integer. Then Equation (13) simplifies as:

$$Q_{\text{sto}}\left(t = k\frac{\pi}{\omega}\right) = V_0 C\left[1 + \exp\left(-\alpha k \frac{\pi}{\omega}\right)\right]. \tag{15}$$

The maximum value of Q_{sto} occurs when $k = 1$. Then, the energy stored in the capacitor bank U_{sto} relative to the energy initially stored in the DEA U_{DEA} is

$$\begin{aligned}\frac{U_{\text{sto}}\left(\frac{\pi}{\omega}\right)}{U_{\text{DEA}}(0)} &= \frac{\frac{1}{2}C_{\text{sto}}^{-1} Q_{\text{sto}}^2\left(\frac{\pi}{\omega}\right)}{\frac{1}{2}C_{\text{DEA}}^{-1} Q_{\text{DEA}}^2(0)} \\ &= \frac{C_{\text{DEA}}}{C_{\text{sto}} Q_{\text{DEA}}^2(0)}\left(V_0 C\left[1 + \exp\left(-\frac{\alpha\pi}{\omega}\right)\right]\right)^2\end{aligned} \tag{16}$$

Letting g be the ratio of the capacitances ${}^{C_{\text{sto}}}/_{C_{\text{DEA}}}$ and substituting $C_{\text{sto}} = gC_{\text{DEA}}$ into Equation (16) and simplifying yields:

$$\frac{U_{\text{sto}}\left(\frac{\pi}{\omega}\right)}{U_{\text{DEA}}(0)} = \frac{g}{(g+1)^2}\left[1 + \exp\left(-\frac{\alpha\pi}{\omega}\right)\right]^2, \tag{17}$$

which is the equation we sought.

Analysis of Equation (17) shows that increasing L increases energy recovery, increasing R_s decreases energy recovery, and there is a value of g that maximizes energy recovery. The effects of L and R_s on energy recovery are contained in the ratio

$$\frac{\alpha}{\omega} = \sqrt{\frac{R_s^2}{4L(1+g)g^{-1}C_{\text{DEA}}^{-1} - R_s^2}}. \tag{18}$$

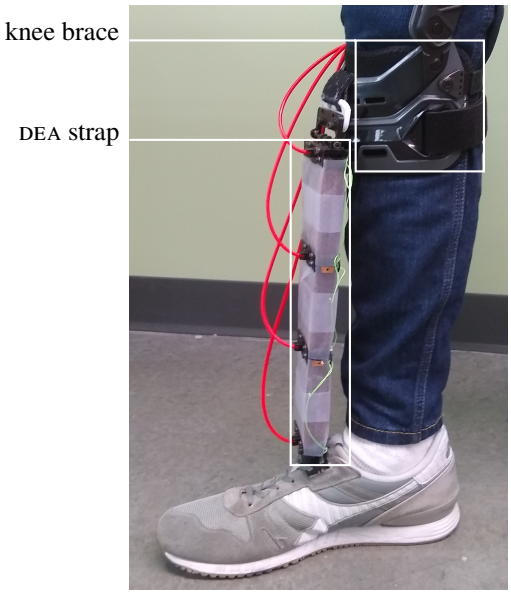

Figure 6: Our DEA AFO prototype consists of a DEA strap that connects a shoe to a knee brace. The control and power electronics (not shown here) would be worn in a waistpack.

Decreasing α/ω makes the circuit less damped and increases the energy recovered according to Equation (17). Increasing L decreases α/ω and increases energy recovery. Increasing R_s increases α/ω and decreases energy recovery. The effect of capacitance ratio g, which determines C_{sto} is more complex. Increasing g increases α/ω and decreases energy recovery. However, the term $g/(g+1)^2$ in Equation (17) has a maximum when $g = 1$. Numerical analysis using values applicable to our charge recovery circuit indicated that optimal charge transfer is obtained for $g \approx 0.9$.

3. Implementation

Our DEA AFO prototype (Figure 6) is designed to counteract foot drop without the drawbacks of AFOs actuated by electric motors, hydraulics, and pneumatics. The DEA strap connects the foot to the shank and provides passive dorsiflexion support. Its foot connector is a 3D-printed component that is laced into a shoe. Its shank connector is a commercial knee brace (MD4200, Elite Bio-Logix, McDavid). The complete design of the AFO would have a pressure-sensitive resistive sensor in the shoe and the control and power electronics worn in a waistpack. The mass of the components currently used is 1.3 kg (Table 2).

The DEA strap is an assembly of 81 individual DEAs (Figure 7). The DEAs are configured in three stacks connected in series mechanically (so that their length changes sum to the total length change), and each stack has 27 DEAs connected in parallel mechanically (so that their forces sum to the total force). The DEAs (Figure 8) use parallel polyimide fibers to maintain a 400 % width prestretch of the VHB 4905 elastomer

Table 2: Mass of DEA AFO components

Component	Mass (kg)	of total
electronics	0.49	38 %
knee brace	0.47	36 %
DEA assembly	0.33	26 %
foot connector	0.01	0 %
Total	1.30	

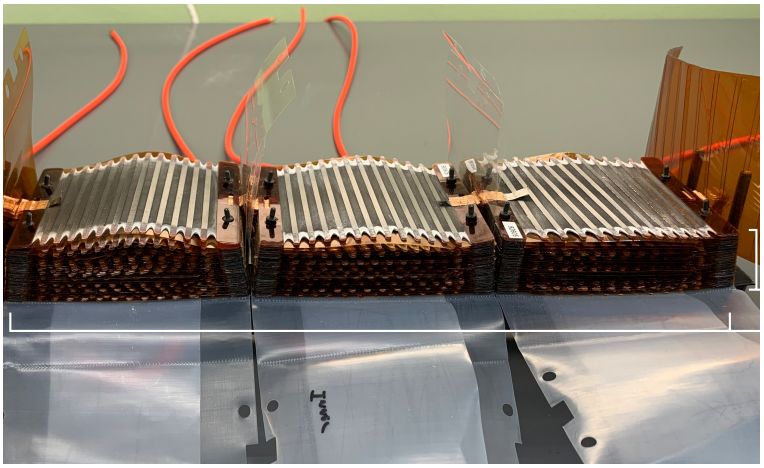

Figure 7: The DEA strap is an assembly of 81 individual DEAs, configured in 3 stacks connected in series mechanically with 27 DEAs connected in parallel mechanically in each stack. This picture depicts a prior version of the DEA strap undergoing assembly before the UHMW polyethylene film was wrapped around the DEAs.

film (made by 3M). Their electrodes are graphite powder (US1058, US Research Nanomaterials), which connect to the electrical supply through leads made of "graphene sheets" (1334N1, McMaster-Carr) and copper tape. The DEAs were fabricated by hand using a process designed to enhance manufacturing precision without the use of expensive manufacturing equipment and dedicated floor space [32]. The DEAs are all connected in parallel electrically so that their capacitances sum to the total capacitance of the assembly. In between the DEAs are pairs of sliding shields made from polyimide film of 50.8 µm (2 mil) thickness. These shields prevent shorting from one DEA around the free edges of the DEA below it to the DEA below that and also protect the DEAs from breakdown arcing of neighboring DEAs in the event of an electrical breakdown. The DEA assembly is wrapped with UHMW polyethylene film of 102 µm (4 mil) thickness to protect humans against electrical shocks.

The AFO's electronics (Figures 5 and 9) are designed to control the voltage on the DEA strap. The electronics are designed to be driven from an 11.1 V lithium polymer battery. A high-voltage DC-DC converter (V_{HV}: FS60P12, XP Power) converts the 11.1 V

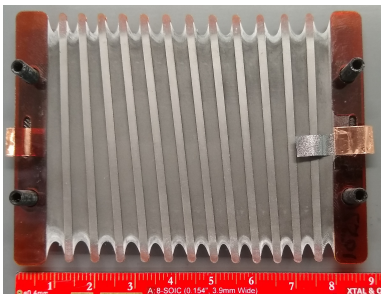

Figure 8: A width-constrained DEA of the type used in the DEA AFO has polyimide fibers that maintain a 400 % width prestretch of the VHB 4905 elastomer film. The DEA is pictured on a storage frame.

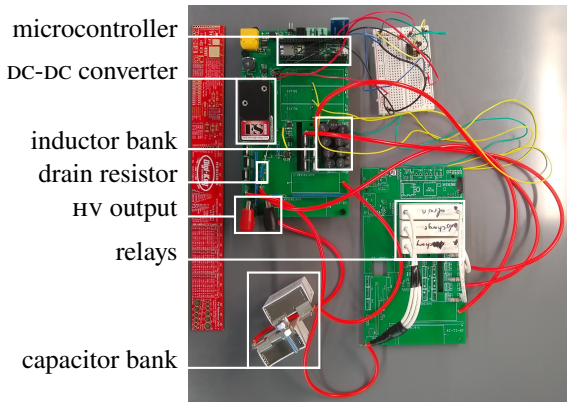

Figure 9: The AFO's power and control electronics.

input to a high voltage (up to 6 kV) for powering the DEA strap. Three high-voltage normally-open relays (S_{ch}, S_{dch}, and S_{dr}: DAT71210F, Cynergy3 Components) route current between the capacitor bank C_{sto}, the drain resistor (R_{dr}), and the DEA strap. The capacitor bank consists of two high-voltage capacitors (C4BSYBX3220ZAFJ, Kemet) connected in series to give a total capacitance of 110 nF. Its purpose is to store the energy that is removed from the DEA strap to make the strap contract until the energy is transferred back to the strap in the next gait cycle. The inductor bank consists of 9 inductors (LHL10TB154J, Taiyo Yuden) connected in series to give a total inductance of 1.35 H. Its purpose is to reduce the energy lost during transfers to and from the capacitor bank. The drain resistor (SM102032004FE-ND, Ohmite) has 2 MΩ of resistance and is used to drain the energy from the DEA strap and the capacitor bank. A microcontroller (Teensy 3.6, PJRC) processes sensor inputs and controls the high-voltage DC-DC converter and relays to operate the AFO.

4. Experimental methods

As a stepping stone before human subject trials, we conducted benchtop tests for preliminary proof of concept. These tests were used to answer several questions:

1. Could the DEA AFO dorsiflex an ankle?
2. Would plantarflexion be easier with the DEA strap charged than with it discharged?
3. How long could the AFO run on a battery?
4. Could charge recovery help it run longer on a battery?

For these benchtop tests, the DEA strap was mounted on a testbed (Figure 10) designed to implement the geometry analyzed in § 2 (Figure 3). The testbed's upright tube is fixed in place, and its lever arm can rotate about the pin joint that represents the ankle. A pair of hard stops limits the lever arm's range of motion to approximately $-20°$ to $10°$ (matching the ankle's range of motion during normal walking). A weight of 7.8 N was suspended from the lever arm at a distance of 6 cm from the ankle joint. This loading is approximately equivalent to 49 % of the ankle torque caused by the foot weight of a person with 800 N body weight. The DEA strap is connected to the testbed with two pin joints. The joint on the upright tube is 35 cm from the ankle joint, and the joint on the lever arm is 5 cm from the ankle joint, matching the values of a and b given near the end of § 2.2. Once the DEA strap was mounted on the testbed, the strap held the lever arm against the upper hard stop. To reduce the effect of viscoelastic stress relaxation on the repeatability of the experiments, the strap was left in this position for about 30 min before the sequence of experiments began. All tests started with the arm resting at the upper hard stop. During the tests, the AFO's microcontroller recorded the voltages on the DEA, capacitor bank, and power input, and the current from the power input at 50 Hz. A video camera recorded the motion of the test bed at 30 Hz, and the arm angle was extracted from these recordings using Tracker video analysis software (`physlets.org/tracker/`) and MATLAB. For the benchtop tests, the AFO's electronics were powered from a benchtop power supply providing 11.1 V in place of a battery.

To determine whether the AFO could dorsiflex an ankle, the lever arm was displaced to the bottom hard stop by hand and then released to see whether it would return to the upper hard stop. In the first test, the arm was released immediately after it reached the bottom hard stop. This test minimized the effect of viscoelastic relaxation on the DEA strap's ability to raise the arm because the DEA strap was fully stretched for only a short time. A second test was run to check whether viscoelastic relaxation would affect the DEA strap's ability to return to the top hard stop. In the second test, the arm was held at the bottom hard stop for 120 s and then released. The longer delay at the bottom hard stop gave more time for viscoelastic relaxation. After being released, the arm was allowed to rise on its own for 90 s, and then it was raised to the upper hard stop by hand and released. The arm was raised by hand and released to check whether friction was a significant factor in preventing the arm from rising fully.

The AFO's ability to ease plantarflexion was tested by charging the DEA strap to 2.8 kV so that it lowered due to the weight of the suspended mass. After the arm reached the bottom hard stop, the DEA was discharged and the arm raised.

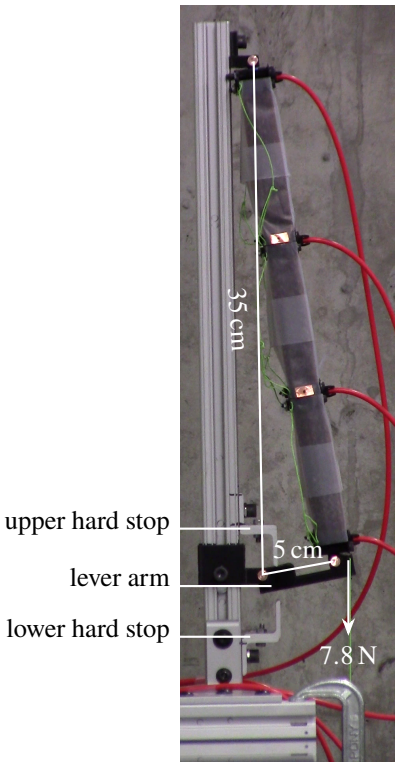

Figure 10: The DEA AFO's testbed connected to the DEA with pin joints [5 and 35] cm from the ankle joint to use the geometry selected during analysis. The motion of the lever arm was constrained by hard stops to approximately $-20°$ to $10°$. The DEA was loaded by a 7.8 N weight connected to the lever arm 6 cm from the ankle joint.

These two tests covered the majority of the loading conditions that the AFO would experience during walking. During foot flat and push off, the AFO would experience imposed displacement, while having a target load of 0 N. This loading condition was simulated by the initial portion of the dorsiflexion tests when the lever arm was pushed down by hand, representing the action of the plantarflexor muscles during push off. The ability of the AFO to exert its target load of 0 N was tested during the plantarflexion test; the lower the force the AFO exerted, the further the lever arm dropped. During swing, the AFO would experience a nearly constant load from the weight of the foot, while having a target displacement of 0°. This loading condition was simulated by the latter portion of the dorsiflexion tests when the lever arm was allowed to rise with the load attached. During loading response, the AFO would experience an increasing load while having a target displacement of 0°. This loading condition was not investigated in this work, but it only occurs during about 8 % of the gait cycle, and the DEA AFO should reduce the severity of foot slap because it provides dorsiflexion support during loading response.

To determine how long the AFO might last on a battery and whether charge recovery could improve the AFO's battery life, the AFO was tested with gait cycle tests that simulated walking with and without charge recovery. In these tests, the AFO's microcontroller operated the DC-DC converter and the relays according to the pattern that would be used during normal walking (Figure 1: Voltage, Relays closed) and the DEA strap cyclically raised and lowered the lever arm. A cycle with charge recovery starts at heel strike with the voltage off and none of the relays closed. Then, at toe contact, the discharge relay is closed to transfer energy from the capacitor bank to the DEA. After a delay to allow the energy to transfer, the voltage is raised to 2.8 kV to charge the DEA so that the lever arm will lower as much as possible. At toe off, the voltage is switched off, the discharge relay is opened, and the charge relay is closed in order to transfer the energy stored on the DEA to the capacitor bank and raise the lever arm. After a delay to allow the energy to transfer, the charge relay is opened, and the drain relay is closed to drain the remaining energy from the DEA so that the lever arm raises as much as possible. A cycle without charge recovery uses the same voltage sequence, but the charge and discharge relays are always open, and the drain relay is closed at toe off instead of later. A single test consisted of 11 continuous cycles, in order to give the system time to reach steady-state operation. The cycles were run on timers instead of being triggered by the toe sensor. Each cycle type was run with two gait periods: 1 s periods to match the pace of normal walking [21], and 5 s periods to allow more time for charging, discharging, and arm motion.

We used the input power measured by the AFO's onboard sensors to estimate how long the AFO would be able to run on a battery. The input power is the product of the input current and input voltage measurements. The total energy consumed during each cycle in the gait cycle tests was calculated by integrating the input power measurement over the gait cycle. To gain more insight into the AFO's power consumption, we measured the power consumed by the electronics with the converter off and all relays open to obtain the power draw of the electronics other than the relays and the converter. This power was multiplied by the gait period to obtain the amount of energy consumed by "other" electronics during each cycle. The power consumed by a single relay was obtained by subtracting the power drawn by other electronics from the power measured

when one relay was closed. The relay power consumption was multiplied by the gait period and the relay duty cycle (portion of the gait period that a relay was active: 20 % with charge recovery inactive, 92 % with charge recovery active) to obtain the energy consumed by relays during each cycle. The energy consumed by the DC-DC converter during each cycle was calculated by subtracting the energy consumed by relays and other electronics from the total energy. The battery life was calculated assuming a 10 W h battery capacity. Such a battery could be an 11.1 V lithium-polymer battery with 900 mA h capacity, which would not be a great burden due to its mass of about 100 g.

We calculated the increase of energy stored on the DEA to assess the performance of the charge recovery system. The energy stored on the DEA U_e can be calculated from the DEA's voltage V_DEA:

$$U_\mathrm{e} = \frac{1}{2} C_\mathrm{DEA} V_\mathrm{DEA}^2. \tag{19}$$

The total increase of energy stored in the DEA during each cycle was calculated from the peak DEA voltage that the converter supplied and the minimum DEA voltage during the gait cycle. The increase of energy contributed by the charge recovery system during each cycle was calculated from the voltage that the capacitor bank charged the DEA to and the minimum DEA voltage during the gait cycle. The capacitance of the DEA C_DEA was calculated by the following procedure. If a switch completes a circuit containing only two capacitors C_1 and C_2, they will both change from their initial voltages, V_{01} and V_{02} respectively, to final voltage V_1. Then the capacitance of one capacitor can be calculated from the capacitance of the other capacitor and the voltage measurements because of the principle of conservation of charge Q:

$$\begin{aligned} Q_0 &= Q_1 \\ C_1 V_{01} + C_2 V_{02} &= C_1 V_1 + C_2 V_2 \\ C_1 V_{01} - C_1 V_1 &= C_2 V_1 - C_2 V_{02} \\ C_1 &= C_2 \frac{V_1 - V_{02}}{V_{01} - V_1}. \end{aligned} \tag{20}$$

The capacitance of the DEA was calculated from Equation (20) using the capacitance of the capacitor bank (110 nF), and the voltages immediately before and after the DEA transferred energy to the capacitor bank during the gait cycle tests with a 5 s gait period yielding $C_\mathrm{DEA} = 133$ nF. This calculation is valid regardless of the resistance in between the capacitors because resistance merely affects the speed of the charge transfer, not the final voltages of the capacitors.

5. Results and discussion

The benchtop test results validate the DEA AFO concept and point to paths for improvement. The DEA AFO can provide dorsiflexion assistance, and charging the DEA assembly reduces the effort that would be required from the plantarflexor muscles to stretch the DEA assembly during push off. However, these capabilities are hampered by the effects of viscoelasticity and friction. The DEA AFO's overall energy consumption

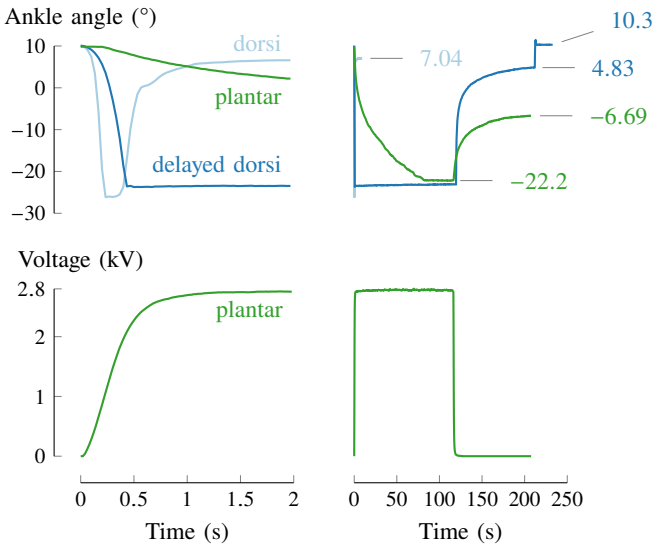

Figure 11: The DEA assembly raised the weighted lever arm after it was manually lowered during the dorsiflexion tests, so the AFO can provide dorsiflexion support. When the DEA assembly was charged to 2.8 kV during the plantarflexion test, it lowered the weighted lever arm to −22.2°, so charging the DEA assembly reduces the effort that would be required from the plantarflexor muscles to stretch the DEA assembly. The left panels show the first 2 s of the tests, and the right panels show the whole tests.

was low enough that it should be able to run for about 7000 steps on a 10 W h battery in actual operation. The charge recovery system was counterproductive in these tests, but it should be beneficial in actual operation. Though the overall AFO concept was sound, a future iteration of the AFO could perform much better with hardware improvements.

5.1. Dorsiflexion and plantarflexion

The DEA AFO can provide dorsiflexion assistance (Figure 11). In the dorsiflexion test, the DEA strap rapidly raised the lever arm and settled at 7.04°. In the delayed dorsiflexion test, the DEA strap raised the lever arm and settled at 4.83°. Then, it was raised to the upper hard stop by hand and released, and it settled at 10.3°. Though the DEA strap did not return the lever arm to its 10° starting angle on its own, these tests showed that the AFO can provide dorsiflexion assistance because the DEA strap raised the weighted lever arm more than 25°.

The DEA AFO's dorsiflexion assistance is hampered by the effects of viscoelasticity and friction (Figure 11). The presence of friction explains why the DEA strap was unable to raise the arm to the upper hard stop. Friction resisted the rising motion of the arm until the DEA strap no longer exerted enough tension to overcome weight and friction and the arm came to rest below the upper hard stop. The lever arm rested at both [4.83 and 10.3]°, which is consistent with the effect of friction on a spring-mass system. A spring-mass system like the test setup has only one equilibrium position—a position where the spring force balances the weight of the mass—if the system is ideal (even with viscous damping). Friction causes a spring-mass system to have an equilibrium zone: a range

of positions where the system can rest because friction is greater than the difference between the spring force and the weight of the mass. Viscoelasticity hampered the DEA strap's ability to raise the lever arm in two ways. First, the motion of the rising lever arm asymptotically decays because this motion is governed by viscoelastic creep, so viscoelasticity slows the dorsiflexion assistance. Second, the lever arm did not rise as high after being held down longer because of viscoelastic stress relaxation, which reduced the tension exerted by the DEA strap on the lever arm and thus its ability to overcome friction.

Charging the DEA strap will make plantarflexion easier than it would be with the DEA strap discharged. If the DEA strap were discharged, the plantarflexor muscles would need to exert effort to stretch it during plantarflexion. In the plantarflexion test, the electric field pressure and the weight of the mass stretched the DEA strap enough to lower the lever arm to $-22.2°$ when the strap was charged to 2.8 kV (Figure 11). Thus, this motion would require no effort from the plantarflexor muscles if the DEA strap were given enough time to stretch due to weight and field pressure. Even when the DEA strap is not given enough time to stretch, the DEA's transduction work will offset the external mechanical work necessary for stretching, so the plantarflexor muscles will need less effort to stretch the DEA strap than they would if the strap were discharged.

In the gait cycle tests (Figure 12), which better represent actual operating conditions than the dorsiflexion and plantarflexion tests, the lever arm traversed a portion of the ankle range of motion. In these tests, the lever arm started at the upper hard stop (10°), lowered when the DEA strap was charged, and raised when the strap was discharged. The arm ended each cycle lower than it started, so it crept downward with successive cycles. However, after the first few cycles, the change in angle in each cycle stabilized and became consistent across cycles. In the trials with a 5 s gait period, the charge and discharge times were much shorter than times allowed for motion in the dorsiflexion and plantarflexion tests. Consequently, the lever arm traversed only a portion of the ankle's range of motion because its speed was limited by viscoelasticity and friction. In the trials with a 1 s gait period, the charge and discharge times were so short that the AFO's electronics could not fully charge and discharge the DEA strap, which further reduced the range of motion. The amount that the arm lowered represents the angular range that would require no effort from the plantarflexor muscle. Motion beyond that range would require some effort from the plantarflexor muscles, but not as much as would be required with the DEA strap discharged. Though the arm drifted lower with successive cycles, this effect is less pronounced for faster motion as seen by comparing the dorsiflexion and delayed dorsiflexion tests (Figure 11). The faster motion of the more realistic 1 s gait period tests indeed shows less drift, and would probably show even less if the electronics were able to fully discharge the DEA in each cycle.

The acoustic noise of the DEA assembly was not measured explicitly, but it was not audible to the ear over the ambient room noise under normal operation such as when trial data was being collected. During development, it occasionally produced faint crackling or whistling noises, but these were associated with DEA breakdown, either incipient or imminent.

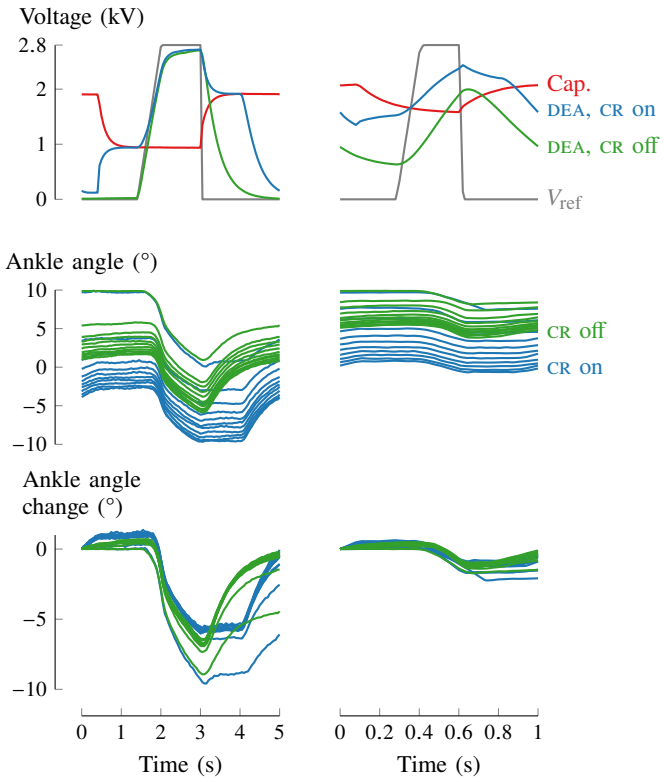

Figure 12: In the gait cycle tests, the voltage and ankle angle trajectories followed regular patterns. The voltages converged to the trajectories depicted here after the first four cycles. The ankle angle crept downward (lower angle) with subsequent cycles, but the ankle angle change was fairly consistent across cycles. Results from trials with a 5 s gait period are shown on the left, and results from trials with a 1 s gait period are shown on the right. CR means charge recovery.

5.2. Energy consumption

In the gait cycle tests, the DEA and capacitor bank voltages followed consistent patterns even though the mechanical motion had not settled to a steady cycle. After the first four cycles, the voltages converged on the trajectories depicted in Figure 12. When the charge recovery system was off, the converter charged the DEA, and then it was drained through the drain resistor. When the charge recovery system was on, the capacitor bank partially charged the DEA, and then the converter charged it to its peak voltage. Then, the charge recovery system recovered a portion of the electrical energy stored on the DEA, and an additional portion was drained through the drain resistor.

The difference between the step estimates for the gait cycle tests with [1 and 5] s gait periods without charge recovery (Table 3, [28 296 and 6991] steps) is caused by two factors. First, the energy consumed by the relays and other electronics is proportional to the gait period so they consumed 5 times more energy in the test with the 5 s gait period than in the test with the 1 s gait period. Second, the energy consumed by the converter is related to the amount of energy supplied to the DEA by the converter, which should have been the same for both tests. However, the combined resistance of the drain resistor and the DEA electrodes prevented the complete discharge of the DEA at the end of the test with a 1 s gait period, so the DEA only received a partial charge from the converter in those tests. Consequently, the converter consumed less energy in the test with the 1 s gait period than in the test with the 5 s gait period.

In actual operation, the DEA AFO's energy consumption should be between that of the tests with the [1 and 5] s gait periods. The relay and other electronics energy consumptions should be similar to those of the tests with the 1 s gait period because those energy consumptions vary with the gait period and the gait period of normal walking is about 1 s [21]. The converter energy consumption should be similar to that of the tests with the 5 s gait period because the DEA was fully charged and discharged during those tests. A refined version of the AFO would have less resistance in the drain circuit so that the DEA would fully discharge during the swing phase of a 1 s gait period and provide maximum dorsiflexion support. It would also use an improved high-voltage supply that would fully charge the DEA during the foot flat phase of a 1 s gait period to allow free plantarflexion during pushoff.

In actual operation, the DEA AFO should be able to run on a battery for about 7000 steps. As explained above, in actual operation, the energy consumed by the relays and other electronics would be similar to the values calculated for the test with a 1 s gait cycle, and the energy consumed by the converter would be similar to the value calculated for the test with a 5 s gait period. Assuming that energy consumed by the relays, other electronics, and converter would be [0.15, 1.22, 3.48] J per cycle respectively, then during actual operation, 4.85 J per cycle would be consumed from the battery, yielding a battery life of 7423 steps.

The charge recovery system was counterproductive in these tests, but it should be beneficial during actual operation. In the gait cycle tests with the charge recovery system on, the capacitor bank contributed to increasing the charge on the DEA, causing the converter to consume less energy (Table 3) than when the charge recovery system was off. But, this benefit was outweighed by the increase of energy consumption by the relays (caused by a relay being active for 92 % of the gait cycle instead of merely

Table 3: Energy consumption results from gait cycle tests and power consumption measured separately

Period (s)	Charge recovery	Power (W)		Energy consumed per cycle (J)				Estimated steps from 10 W h battery	Increase of energy stored in DEA per cycle		
		Relay	Other	Total	Relay	Other	Converter		Total (mJ)	From cap. bank (mJ)	(%)
5	off	0.74	1.22	10.30	0.74	6.08	3.48	6991	487	0	0
	on			11.78	3.40	6.08	2.29	6114	490	58	12
1	off			2.54	0.15	1.22	1.18	28296	212	0	0
	on			2.88	0.68	1.22	0.98	24997	253	33	13

20 %, see Figure 1), which caused the total energy consumption to be greater than when the charge recovery system was off. As explained above, in actual operation, the energy consumed by the relays and other electronics would be similar to the values calculated for the test with a 1 s gait cycle, and the energy consumed by the converter would be similar to the value calculated for the test with a 5 s gait period. Thus, the increase in energy consumption from the relays should be about 0.53 J per cycle as seen in the tests with the 1 s gait period. And, the decrease of energy consumption by the converter should be about 1.19 J per cycle as seen in the tests with the 5 s gait period. Therefore, in actual operation, the charge recovery system should reduce the total energy consumption by about 0.66 J per cycle.

5.3. Improving performance

The viscoelasticity that slowed dorsiflexion and plantarflexion could be mitigated by applying higher voltages or changing the DEAs' elastomer. The effect of viscoelasticity on dorsiflexion may not be significant during actual operation because the DEA assembly would be stretched and released quickly (Figure 1) like in the dorsiflexion test (Figure 11). The effect of viscoelasticity on plantarflexion could be compensated for by "overdriving" the DEA assembly with a higher voltage for the brief push off period [33]. This approach may be practical because DEAs can withstand higher voltages for brief periods [34]. Alternatively, the effects of viscoelasticity could be dramatically reduced by redesigning the DEAs around a silicone elastomer, which would have much less viscoelasticity than the VHB 4905 currently used [35, 36]. VHB 4905 has a glass transition range from −50 °C to 60 °C [37]. At room temperature, the operating condition for the experiments in this work, VHB 4905 has highly dissipative stress-strain behavior with $\tan\delta \approx 1$ [37]. This dissipation prevents potential energy (either gravitational when the mass was raised or elastic when the arm was lowered) from being converted into kinetic energy of the moving mass and thus hinders rapid movement. In contrast, silicone elastomers suited for DEAs typically have glass transitions below −100 °C, so at room temperature, they are in their rubbery state with viscous effects that are nearly negligible, with $\tan\delta \approx 0.01$ [36]. With these properties, the DEAs would dissipate almost no potential energy so the kinetic energy of the mass would be much greater, and the lever arm would raise and lower much faster.

Using a silicone instead of VHB 4905 would also mitigate two other detrimental effects of viscoelasticity: temperature-dependent behavior and a "warm-up" time. The stress-strain behavior of VHB 4905 is highly temperature-dependent [38] within its glass transition range: it softens with increasing temperature and stiffens with decreasing temperature. In contrast, silicones suited for DEAs stay in their rubbery state for a wide temperature range around room temperature and have stress-strain behavior that is much less temperature-dependent. The viscoelastic nature of VHB 4905 means that in real-world use, if the DEA assembly was allowed to relax to its rest length, such as might occur if the AFO was doffed and set aside over night, then when the AFO was donned, the DEA assembly would exert a stronger dorsiflexion force than normal until it relaxed into its operating length. This effect would mean the wearer would have to exert additional plantarflexion effort during the relaxation period, which is on the order of a few minutes. This effect could be mitigated by storing the DEA assembly on a frame that held it at the operating length when not in use. Alternatively, using an appropriate silicone for the DEA elastomer would almost entirely eliminate the issue because the silicone's stress-strain behavior would have minimal dependence on strain history due to the material's low value of $\tan\delta$.

In itself, reducing viscoelasticity would not have significantly reduced the AFO's energy consumption in these tests, but it may do so for future iterations. In the tests in this work, the AFO was controlled with open-loop control that did not account for the effects of viscoelasticity, so it expended no extra energy because of viscoelasticity. The major effects of viscoelasticity were to slow the motion of the lever arm in dorsiflexion and to reduce the AFO's ability to ease plantarflexion as explained in § 5.1. Had there been no viscoelasticity, the ankle angle change observed in the gait cycle tests (Figure 12) may have been greater, and this would have increased energy consumption because the DEA strap's capacitance increases as it elongates. This effect would have been minor because the capacitance only increases by about 21 % when the lever arm goes from the upper hard stop to the lower hard stop. However, if the lever arm angle or the AFO's output force was modulated with closed-loop control, then reducing the viscoelasticity of the DEA elastomer could reduce energy expended in tracking the reference trajectories.

The energy consumption of the DEA AFO could be reduced by improving the charge recovery system.[1] The charge recovery system's energy consumption could be lowered by replacing the relays with high-voltage transistors, which would consume much less power to activate. Additionally, the energy saved by the charge recovery system could be increased by adding inductance or decreasing DEA electrode resistance to make the charge transfer more effective. Currently, the charge recovery system has only 1.35 H of inductance. According to Equation (12), the charge recovery system should have

$$L > \frac{R_s^2 C}{4} = \frac{(860\,\mathrm{k\Omega})^2 \cdot 60.2\,\mathrm{nF}}{4} = 11.1\,\mathrm{kH} \tag{21}$$

to be underdamped, which would allow it recover more than 25 % of the electrical

[1] Of course, the AFO's energy consumption could also be improved by refining the low-voltage circuitry that consumes a significant amount of energy itself.

energy stored in the DEA assembly.[2] Alternatively, if the DEA electrode resistance was made negligible by using metallic electrodes, and only the parasitic resistance of the inductor bank (2.7 kΩ) affected the charge transfer, then

$$L > \frac{R_s^2 C}{4} = \frac{(2.7\,\mathrm{k\Omega})^2 \cdot 60.2\,\mathrm{nF}}{4} = 0.11\,\mathrm{H} \tag{22}$$

would make the system underdamped. Further, substituting $R_s = 2.7\,\mathrm{k\Omega}$, $L = 1.3\,\mathrm{H}$, $C_{DEA} = 133\,\mathrm{nF}$, and $g = 0.8721$ into Equations (17) and (18) yields an energy recovery of 48 %.

Refining the AFO's design could reduce the AFO's mass significantly. The mass of the DEA assembly is merely 26 % of the entire AFO mass (Table 2). The majority of the mass is in the electronics and knee brace, and these components were not optimized. The electronics would probably have less mass if consolidated into a single circuit board, and the knee brace's mass could probably be reduced by replacing the off-the-shelf brace with a custom design tailored for the needs of the AFO.

Adding additional DEAs to the assembly would strengthen it to bear the full weight of a foot. In these tests, the DEA assembly supported approximately 49 % of the ankle torque caused by foot weight. Because ankle dorsiflexor weakness can range from slight to total [39], this partial support may be useful to a foot drop patient with partial dorsiflexor function. For the full support required by foot drop patients with no dorsiflexor function, the DEA assembly could be strengthened by adding additional DEAs in parallel mechanically. Doing so would scale the assembly's strength linearly with the number of additional parallel DEA layers, and would be only a minor design revision. The additional DEAs would increase the assembly's capacitance and decrease its resistance, so the power supply and charge recovery components would have to be reselected accordingly.

6. Conclusion

Our DEA AFO design promises to relieve foot drop symptoms with less mass, noise, and energy consumption than electric and pneumatic powered AFOs. It can provide dorsiflexion support, which will help relieve toe drag and foot slap. It can also reduce the effort required from plantarflexor muscles to stretch the DEA assembly, so future iterations may allow nearly free plantarflexion during push off, unlike common passive AFOs. It is currently comparable to the lighest powered AFOs in mass, but its mass can be reduced because much of that mass is in unoptimized components. It operates silently, so it is quieter than electric and pneumatic powered AFOs. Its energy consumption was low enough that the AFO should be able to run for 7000 steps, enough for a full day of walking, on a small battery. We expect that after the toe contact sensor is installed, the electronics are installed in a waistpack, and the design is further refined, the DEA AFO should be able to demonstrate these benefits in human subject trials.

[2] For this calculation, R_s was determined from the RC time constant obtained from a logarithmic curve fit of the voltage decay while the DEA assembly discharged across R_{dr}.

Beyond relieving foot drop symptoms, the DEA AFO demonstrates the potential of DEAs to transform powered prostheses and orthoses. DEAs have the force and stretch capacity to directly drive joints without reduction transmissions, which leads to designs with less weight and bulk. They operate silently making the prosthesis or orthosis less obtrusive to its wearer. Additionally, their compliance and flexibility facilitates designs that conform more closely to the body or are more natural in appearance. We anticipate that these characteristics will be beneficial for other powered prostheses and orthoses as well, opening the door to a new generation of assistive devices that restore human mobility in a more lifelike fashion.

Acknowledgements

The authors gratefully acknowledge the assistance of the following individuals in completing this project:

Andrew Glick for assistance in prototyping and in fabricating DEAs,

Mark Allen for assistance in fabricating DEAs,

Wayne Henricks for assistance in designing the DEA's high-voltage power system.

Funding: This work was partially supported by the National Science Foundation under award 1830360/1953908. R. D. Gregg holds a Career Award at the Scientific Interface from the Burroughs Wellcome Fund. W. Voit acknowledges support from the DARPA Young Faculty Award, the DARPA Director's Fellowship (No. D13AP00049), and the Center for Engineering Innovation.

References

[1] J. Farley, Controlling drop foot: Beyond standard AFOs, Lower Extremity Review (oct 2009).
URL http://lermagazine.com/article/controlling-drop-foot-beyond-standard-afos

[2] J. A. Blaya, H. Herr, Adaptive Control of a Variable-Impedance Ankle-Foot Orthosis to Assist Drop-Foot Gait, IEEE Transactions on Neural Systems and Rehabilitation Engineering 12 (1) (2004) 24–31. doi:10.1109/TNSRE.2003.823266.

[3] U. Martinez-Hernandez, A. Rubio-Solis, V. Cedeno-Campos, A. A. Dehghani-Sanij, Towards an intelligent wearable ankle robot for assistance to foot drop, in: IEEE International Conference on Systems, Man and Cybernetics, IEEE, 2019, pp. 3410–3415. doi:10.1109/SMC.2019.8914170.
URL https://ieeexplore.ieee.org/document/8914170/

[4] L.-F. Yeung, C. Ockenfeld, M.-K. Pang, H.-W. Wai, O.-Y. Soo, S.-W. Li, K.-Y. Tong, Design of an exoskeleton ankle robot for robot-assisted gait training of stroke patients, in: IEEE International Conference on Rehabilitation Robotics,

IEEE, 2017, pp. 211–215. doi:10.1109/ICORR.2017.8009248.
URL http://ieeexplore.ieee.org/document/8009248/

[5] L.-F. Yeung, C. Ockenfeld, M.-K. Pang, H.-W. Wai, O.-Y. Soo, S.-W. Li, K.-Y. Tong, Randomized controlled trial of robot-assisted gait training with dorsiflexion assistance on chronic stroke patients wearing ankle-foot-orthosis, Journal of NeuroEngineering and Rehabilitation 15 (1) (2018) 51. doi:10.1186/s12984-018-0394-7.
URL https://jneuroengrehab.biomedcentral.com/articles/10.1186/s12984-018-0394-7

[6] K. A. Shorter, G. F. Kogler, E. Loth, W. K. Durfee, E. T. Hsiao-Wecksler, A portable powered ankle-foot orthosis for rehabilitation, The Journal of Rehabilitation Research & Development 48 (4) (2011) 459–472. doi:10.1682/JRRD.2010.04.0054.
URL http://www.rehab.research.va.gov/jour/11/484/pdf/shorter484.pdf

[7] M. K. Boes, M. Islam, Y. David Li, E. T. Hsiao-Wecksler, Fuel efficiency of a Portable Powered Ankle-Foot Orthosis, in: IEEE International Conference on Rehabilitation Robotics, IEEE, 2013, pp. 1–6. doi:10.1109/ICORR.2013.6650445.
URL http://ieeexplore.ieee.org/document/6650445/

[8] K. A. Shorter, Y. Li, T. Bretl, E. T. Hsiao-Wecksler, Modeling, control, and analysis of a robotic assist device, Mechatronics 22 (8) (2012) 1067–1077. doi:10.1016/j.mechatronics.2012.09.002.
URL http://dx.doi.org/10.1016/j.mechatronics.2012.09.002

[9] G. M. Gu, S. Kyeong, D.-S. Park, J. Kim, SMAFO: Stiffness modulated Ankle Foot Orthosis for a patient with foot drop, in: IEEE International Conference on Rehabilitation Robotics, IEEE, 2015, pp. 543–548. doi:10.1109/ICORR.2015.7281256.
URL http://ieeexplore.ieee.org/document/7281256/

[10] S. J. Kim, H. Chang, J. Park, J. Kim, Design of a Portable Pneumatic Power Source With High Output Pressure for Wearable Robotic Applications, IEEE Robotics and Automation Letters 3 (4) (2018) 4351–4358. doi:10.1109/LRA.2018.2864823.
URL https://ieeexplore.ieee.org/document/8430733/

[11] S. H. Collins, M. B. Wiggin, G. S. Sawicki, Reducing the energy cost of human walking using an unpowered exoskeleton, Nature 522 (2015) 212–215. doi:10.1038/nature14288.
URL http://dx.doi.org/10.1038/nature14288http://www.nature.com/articles/nature14288

[12] M. B. Yandell, J. R. Tacca, K. E. Zelik, Design of a Low Profile, Unpowered Ankle Exoskeleton That Fits Under Clothes: Overcoming Practical Barriers to

Widespread Societal Adoption, IEEE Transactions on Neural Systems and Rehabilitation Engineering 27 (4) (2019) 712–723. doi:10.1109/TNSRE.2019.2904924.

[13] S. Diller, C. Majidi, S. H. Collins, A Lightweight, Low-Power Electroadhesive Clutch and Spring for Exoskeleton Actuation, in: IEEE International Conference on Robotics and Automation, IEEE, Stockholm, 2016, pp. 682–689. doi:10.1109/ICRA.2016.7487194.
URL https://ieeexplore.ieee.org/document/7487194

[14] J. Furusho, T. Kikuchi, M. Tokuda, T. Kakehashi, K. Ikeda, S. Morimoto, Y. Hashimoto, H. Tomiyama, A. Nakagawa, Y. Akazawa, Development of Shear Type Compact MR Brake for the Intelligent Ankle-Foot Orthosis and Its Control; Research and Development in NEDO for Practical Application of Human Support Robot, in: IEEE International Conference on Rehabilitation Robotics, IEEE, 2007, pp. 89–94. doi:10.1109/ICORR.2007.4428411.
URL http://ieeexplore.ieee.org/document/4428411/

[15] W. Svensson, U. Holmberg, Ankle-Foot-Orthosis Control in Inclinations and Stairs, in: IEEE Conference on Robotics, Automation and Mechatronics, IEEE, 2008, pp. 301–306. doi:10.1109/RAMECH.2008.4681479.
URL http://ieeexplore.ieee.org/document/4681479/

[16] H. M. Herr, R. D. Kornbluh, New horizons for orthotic and prosthetic technology: artificial muscle for ambulation, in: Proceedings of SPIE (EAPAD), Vol. 5385, 2004, pp. 1–9. doi:10.1117/12.544510.
URL http://link.aip.org/link/?PSI/5385/1/1{&}Agg=doi{%}5Cnhttp://biomech.media.mit.edu/publications/ArtificialMuscle{_}O{&}P.pdf

[17] A. P. Mulgaonkar, R. Kornbluh, H. Herr, A new frontier for orthotics and prosthetics: Application of dielectric elastomer actuators to bionics, in: F. Carpi, D. De Rossi, R. Kornbluh, R. Pelrine, P. Sommer-Larsen (Eds.), Dielectric Elastomers as Electromechanical Transducers, 2008, Ch. 19, pp. 189–206. doi:10.1016/B978-0-08-047488-5.00019-8.

[18] R. Pelrine, R. D. Kornbluh, Electromechanical Transduction Effects in Dielectric Elastomers: Actuation, Sensing, Stiffness Modulation and Electric Energy Generation, in: F. Carpi, D. De Rossi, R. D. Kornbluh, R. Pelrine, P. Sommer-Larsen (Eds.), Dielectric Elastomers as Electromechanical Transducers, Elsevier Science, 2008, Ch. 1, pp. 3–12. doi:10.1016/B978-0-08-047488-5.00001-0.
URL https://www.sciencedirect.com/science/article/pii/B9780080474885000010

[19] D. Allen, E. Bolívar, S. Farmer, W. Voit, R. D. Gregg, Mechanical simplification of variable-stiffness actuators using dielectric elastomer transducers, Actuators 8 (2019).

[20] J. Vincent, Basic Elasticity and Viscoelasticity, in: Structural Biomaterials, 3rd Edition, Princeton University Press, 2012, Ch. 1, pp. 1–28.
URL http://assets.press.princeton.edu/chapters/s9774.pdf

[21] J. Perry, J. M. Burnfield, L. Cabico, Gait Analysis: Normal and Pathological Function, 2nd Edition, Slack, Thorofare, NJ, 2010.

[22] D. A. Winter, Biomechanics and motor control of human gait: normal, elderly and pathological, 1991.

[23] D. Allen, Design principles for using dielectric elastomer transducers applied to powered prostheses and orthoses (2020).

[24] D. Wang, The Most Energy Efficient Way to Charge the Capacitor in a RC Circuit, Physics Education 52 (6) (2017) 065019. doi:10.1088/1361-6552/aa8973.
URL http://stacks.iop.org/0031-9120/52/i=6/a=065019?key=crossref.ac1f7a2a301b55eabd0124c914f75444

[25] D. Quintero, D. J. Villarreal, D. J. Lambert, S. Kapp, R. D. Gregg, Continuous-phase control of a powered knee–ankle prosthesis: Amputee experiments across speeds and inclines, IEEE Transactions on Robotics 34 (3) (2018) 686–701. doi:10.1109/TRO.2018.2794536.

[26] M. A. Holgate, T. G. Sugar, A. W. Bohler, A novel control algorithm for wearable robotics using phase plane invariants, in: 2009 IEEE International Conference on Robotics and Automation, 2009, pp. 3845–3850. doi:10.1109/ROBOT.2009.5152565.

[27] R. W. Bohannon, Number of Pedometer-Assessed Steps Taken Per Day by Adults: A Descriptive Meta-Analysis, Physical Therapy 87 (12) (2007) 1642–1650. arXiv:https://academic.oup.com/ptj/article-pdf/87/12/1642/9410129/ptj1642.pdf, doi:10.2522/ptj.20060037.
URL https://doi.org/10.2522/ptj.20060037

[28] J.-P. L. Bigué, J.-S. Plante, Experimental Study of Dielectric Elastomer Actuator Energy Conversion Efficiency, IEEE/ASME Transactions on Mechatronics 18 (1) (2013) 169–177. doi:10.1109/TMECH.2011.2164930.
URL http://ieeexplore.ieee.org/ielx5/3516/6301724/06022797.pdf?tp={&}arnumber=6022797{&}isnumber=6301724{%}0Ahttp://ieeexplore.ieee.org/xpls/abs{_}all.jsp?arnumber=6022797{&}tag=1http://ieeexplore.ieee.org/document/6022797/

[29] H. C. Lo, T. Gisby, E. Calius, I. Anderson, Transferring electrical energy between two dielectric elastomer actuators, Sensors and Actuators, A: Physical 212 (2014) 123–126. doi:10.1016/j.sna.2014.03.020.
URL http://dx.doi.org/10.1016/j.sna.2014.03.020

[30] H. C. Lo, Converters for Milliwatt Dielectric Elastomer Generators, Ph.d. dissertation, University of Auckland (2015).
URL http://hdl.handle.net/2292/27120

[31] A. K. Singal, The Paradox of Two Charged Capacitors – A New Perspective, Physics Education 31 (4) (2015).
URL http://www.physedu.in/pub/Oct-Dec-2015/PE15-07-315

[32] R. Little, Manufacturing methods for medium-volume production of planar dielectric elastomer actuators (2020).

[33] A. Poulin, S. Rosset, An open-loop control scheme to increase the speed and reduce the viscoelastic drift of dielectric elastomer actuators, Extreme Mechanics Letters 27 (2019) 20–26. doi:10.1016/j.eml.2019.01.001.
URL https://linkinghub.elsevier.com/retrieve/pii/S2352431618302360https://doi.org/10.1016/j.eml.2019.01.001

[34] T. Kobayashi, S. K. Smoukov, Pulsed actuation avoids failure in dielectric elastomer artificial muscles, International Journal of Smart and Nano Materials 5 (4) (2014) 217–226. doi:10.1080/19475411.2014.987190.
URL http://www.tandfonline.com/doi/abs/10.1080/19475411.2014.987190

[35] R. D. Kornbluh, R. Pelrine, High-Performance Acrylic and Silicone Elastomers, in: F. Carpi, D. De Rossi, R. Kornbluh, R. Pelrine, P. Sommer-Larsen (Eds.), Dielectric Elastomers as Electromechanical Transducers, Elsevier Science, 2008, Ch. 4, pp. 33–42. doi:10.1016/B978-0-08-047488-5.00004-6.
URL http://linkinghub.elsevier.com/retrieve/pii/B9780080474885000046

[36] F. B. Madsen, A. E. Daugaard, S. Hvilsted, A. L. Skov, The Current State of Silicone-Based Dieletric Elastomer Transducers, Macromolecular Rapid Communications 37 (2016) 378–413. doi:10.1002/marc.201500576.
URL https://onlinelibrary.wiley.com/doi/full/10.1002/marc.201500576

[37] J. Sheng, H. Chen, J. Qiang, B. Li, Y. Wang, Thermal, Mechanical, and Dielectric Properties of a Dielectric Elastomer for Actuator Applications, Journal of Macromolecular Science, Part B 51 (10) (2012) 2093–2104. doi:10.1080/00222348.2012.659617.
URL https://www.tandfonline.com/doi/full/10.1080/00222348.2012.659617

[38] Z. Liao, M. Hossain, X. Yao, M. Mehnert, P. Steinmann, On thermo-viscoelastic experimental characterisation and numerical modelling of VHB polymer, International Journal of Non-Linear Mechanics 118 (2020) 103263. doi:10.1016/j.ijnonlinmec.2019.103263.
URL https://doi.org/10.1016/j.ijnonlinmec.2019.103263

[39] A. Ghahreman, R. D. Ferch, P. Rao, N. Chandran, B. Shadbolt, Recovery of ankle dorsiflexion weakness following lumbar decompressive surgery, Journal of Clinical Neuroscience 16 (8) (2009) 1024 – 1027. doi:https://doi.org/10.1016/j.jocn.2008.10.017.

URL http://www.sciencedirect.com/science/article/pii/S0967586808006139